High-Efficiency Plasma Refuelling by Pellet Injection from the Magnetic High-Field Side into ASDEX Upgrade

P. T. Lang, K. Büchl, M. Kaufmann, R. S. Lang, V. Mertens, H. W. Müller, J. Neuhauser, ASDEX Upgrade, and NI Teams
Max-Planck-Institut für Plasmaphysik, EURATOM-IPP Association, Garching, Germany
(Received 25 September 1996)

High-efficiency refuelling of ELMy *H*-mode tokamak discharges with solid deuterium pellets injected from the magnetic high-field side is demonstrated. Compared to standard low-field side injection, the fuelling efficiency was enhanced by a factor of 4, the pellet penetration more than 2 times. This experimental result can be qualitatively explained by the magnetic force pushing a diamagnetic plasma cloud towards lower magnetic field, causing rapid particle loss for shallow low-field side injection, but enhancing fuelling efficiency and pellet penetration for high-field side injection. [S0031-9007(97)03857-X]

PACS numbers: 28.52.Cx, 52.55.Fa

Next generation fusion devices like ITER will have to operate at densities well beyond the Greenwald limit obtained in present day tokamaks with gas refuelling [1]. Though the detailed nature of this empirical limit is still under discussion, it was shown that it can easily be overcome by injection of frozen hydrogen isotope pellets penetrating much deeper than cold gas particles (e.g., Franck-Condon atoms from molecule disintegration) [2]. In discharges with high heating power and especially in type-I ELMy *H*-mode plasmas with high edge temperatures, a large fraction of the deposited material was rapidly expelled from the plasma column [3], resulting in significantly reduced fuelling efficiencies ε_f especially with shallow penetration [2,4]. In Ref. [4] it was shown that at least part of this mass was lost in the vicinity of the injection point along a trace aligned with the helical magnetic field (please note the correct sequence of Figs. 3(a) and 3(b) is reproduced in the corrigendum).

In this and all previous experiments, pellets were injected from the magnetic low-field side (LFS), i.e., from the torus outside, which is easily accessible in a tokamak. It was therefore argued [4] that, because of the unfavorable toroidal curvature, part of the diamagnetic pellet plasma cloud could have been expelled before it was captured by the background plasma. If so, injection from the magnetic high-field side (HFS), i.e., the torus inside, should be much superior, since the same effect would help to transport the pellet mass deeper into the bulk plasma. In order to clarify this question, experiments have been conducted in ASDEX Upgrade where pellets were injected from both sides into *H*-mode plasmas and ε_f as well as pellet penetration depths were compared.

ASDEX Upgrade is a midsize divertor tokamak (tokamak radius $R_0 = 1.65$ m, plasma radius $a = 0.5$ m, $V_{\text{plasma}} = 13$ m^3, plasma elongation $b/a = 1.6$; single-null divertor). Wall elements in contact with the plasma are covered by graphite tiles, the divertor target plates were tungsten coated. Calibrated valves mounted at the vessel midplane are used for gas puffing, and turbomolecular pumps with a pumping speed of 14 m^3/s for D_2 (deuterium) gas to control particle exhaust.

The experiments described here were carried out in D with plasma currents $I_p = 0.8$–1.2 MA, toroidal magnetic field $|B_t| = 1.7$–2.5 T, safety factor $q_{95} = 2.7$–4.2, and additional beam injection heating of up to 7 MW for H^0 (Hydrogen) and up to 10 MW for D^0 injection.

Pellet ablation is monitored by a CCD camera (Fig. 1) and photodiodes. Video pictures showing the ablation zone of the pellets are used to estimate the pellet penetration depths. A DCN interferometer, a Li-beam system, a Thomson scattering system, and an ECE radiometer are applied to measure the density profile and determine the plasma particle content; the latter two are also used for temperature profile investigations. Further diagnostics are

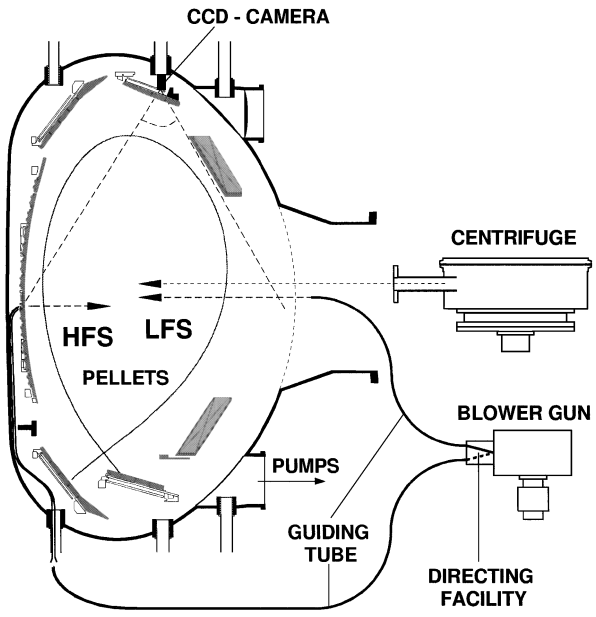

FIG. 1. Cross section of the ASDEX Upgrade divertor tokamak. Pellet injection is performed by the centrifuge or via guiding tubes by the blower gun. A CCD camera is installed for pellet observation.

bolometer cameras, Langmuir probes in the target plates, fast target plate thermography, reflectometry, neutral gas gauges, and Mirnov coils.

Pellet injection is performed either with a centrifuge injector or a blower gun (Fig. 1). The centrifuge injects only from the LFS. D_2 pellets of variable velocity (240 to 1200 m/s) and mass (1.4 to 3.8 $\times$ 10^{20} particles) can be delivered at repetition rates of up to 80 Hz. The blower gun injects D_2 pellets containing 3 $\times$ 10^{20} particles, accelerated by H_2 gas flow of up to 130 m/s at repetition rates of up to 17 Hz. Pellets are delivered via guiding tubes optionally from the magnetic low- or high-field side.

The measured increase of the number of particles in the target plasma (1–2 ms after ablation) divided by the number of particles contained in the pellet is defined as fuelling efficiency ε_f. To calculate ε_f we used the maximum pellet mass found in test bed shots at the exit of the injectors, including the guiding tubes. Thus, the calculated values systematically underestimate ε_f. In the case of HFS injection, mass losses enhanced with respect to test bed values can occur in the experiment due to coupling of inner and outer guiding tubes. As these losses may strongly differ for different pellets, they cause strong scatter of ε_f in the case of HFS injection.

To demonstrate the enhanced refuelling performance of HFS pellets, LFS and HFS pellets were injected into the same plasma discharge under practically identical conditions. Figure 2 shows the temporal evolution of such a discharge ($I_p = 0.8$ MA, $B_t = -1.9$ T, $q_{95} = 3.6$, neutral beam heating power $P_{\mathrm{NI}} = 7.5$ MW). During the whole sequence the discharge maintained type-I ELMy *H*-mode behavior. Gas puffing was initially applied to control the line-averaged density at the required value of 7 $\times$ 10^{19} m^{-3}. The LFS pellet injection sequence was started after the density reached the preprogrammed value, and the HFS sequence was applied about 0.5 s after termination of the LFS pellet sequence, when the discharge had returned to identical starting conditions. Both sequences consisted of a nominal 10 pellets each with the same, relatively small, nominal velocity of 130 m/s. A strong enhancement of ε_f with the HFS pellets in relation to the LFS pellets can already be concluded from the increase in line-averaged density. The ε_f with the HFS pellets are about 4 times as high as the values obtained for LFS pellets. The higher efficiency with HFS pellets is also obvious from the particle flux applied as D_2 gas puff or D_2 pellets injected to the plasma. Pellets launched into the plasma are monitored by the spikes they cause in the D_α radiation. The total amount of radiation can be assumed to yield an approximate measure of the deposited pellet mass [5]. Reduced intensities observed with some pellets are most probably due to mass losses on the external pellet path. The nominal pellet sequence yields the average nominal particle flux shown in Fig. 2. Whereas additional gas input is required by the plasma control system during the LFS sequence to reach the preset line density, gas valves close almost immediately

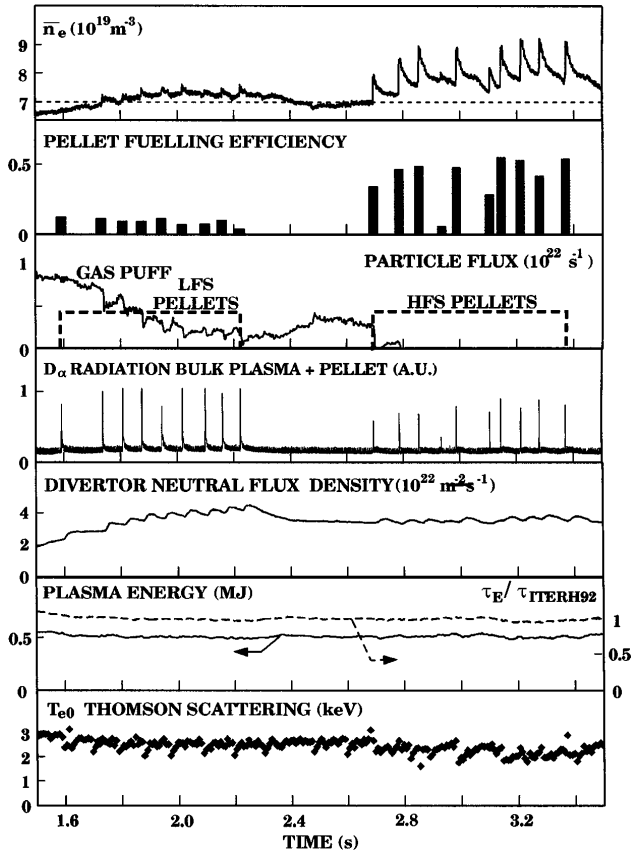

FIG. 2. Temporal evolution of a discharge with LFS and HFS pellet injection applied under identical pellets and plasma starting conditions.

after the start of the HFS pellet train. The divertor neutral flux density Γ_0^{div} gradually increases during the LFS sequence, whereas an almost constant lower value is maintained during the HFS sequence. With HFS pellet injection, significant density increase is achieved without deterioration of the plasma energy or energy confinement time τ_E. With LFS pellet injection, in contrast, no comparable density increase is observed. In earlier LFS experiments [6], density enhancement similar to that with present HFS injection was achieved only with 80 Hz pellet injection yielding approximately 6 times higher particle flux. This enhancement was always accompanied by a loss of plasma energy, a reduction of τ_E and strong cooling of the plasma. During HFS injection no drastic reduction of the electron temperature T_e occurs; the modest decrease of T_{e0} shown in Fig. 2 is due to the density increase since the stored energy is not altered.

In addition to the direct comparison between LFS and HFS injection in the same discharge, a series of pellet injections was performed under various plasma conditions. Figure 3 shows ε_f values for different P_{NI}. For $P_{\mathrm{NI}} >$ 5 MW HFS pellets (filled symbols) showed efficiencies enhanced by up to 4 times that with equivalent LFS pellets (open symbols). With increasing P_{NI} and plasma temperature, HFS pellets show no significant power degra-

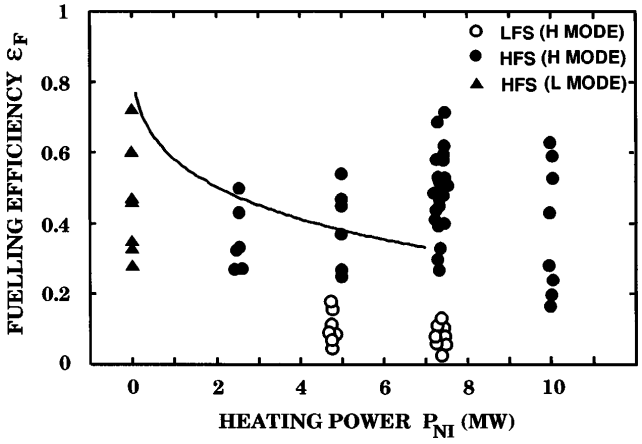

FIG. 3. The triangles and circles show the fuelling efficiency calculated on the assumption of maximum pellet masses versus additional heating power for LFS (open symbols) and HFS (filled symbols) pellets injected with the blower gun. Triangles: pellets into Ohmic or *L*-mode plasmas; circles: *H*-mode target plasmas. The solid line represents the upper limit of fuelling efficiency in the case of LFS injection performed by the centrifuge.

dation of ε_f, whereas the maximum efficiency achieved using LFS pellets (solid line) is dropping. Even at the highest heating powers applied almost the same efficiencies are achieved for HFS pellets as in Ohmic plasmas. The strong scatter of ε_f values is most probably an artifact caused by the external pellet mass losses mentioned earlier. This conclusion is further supported by the fact that reduced ε_f values were always accompanied by reduced ablation radiation. With the ablation radiation being assumed to be a good measure of the pellet mass [5], accordingly corrected ε_f values show a scatter reduced to $\pm 10\%$ of the optimum value of ≈ 0.7 for the HFS pellets. For LFS pellets, however, a strong reduction in efficiency takes place despite the fact even bigger (4×10^{20} particles) and faster (1200 m/s) pellets were injected using the centrifuge at high heating powers, penetrating deep into the plasma. In the case of shallow penetration into type-I ELMy *H*-mode plasmas ε_f was even restricted to values below 0.2 [4]. Comparable conditions yielded the same result in the case of LFS pellet injection with the blower gun, as shown in Fig. 3. Ejection of material was, in fact, observed by reflectometry, Langmuir probes, and thermography. Obviously, immediately after ablation and in parallel to the toroidal expansion, there is fast outward radial transport on a time scale less than 1 ms. Such outward flow of particles was first reported from JET and TFTR [7]. Like in those experiments, also analysis of our LFS pellet injection experiments showed increasing outward shift of the deposition profile measured a few ms after pellet injection with respect to the dynamic ablation profile obtained by the ablation radiation for increasing P_{NI}. This radial transport strongly increases as the plasma temperature and hence as P_{NI}. In the case of strong auxiliary heating, video observations near the pellet injection port showed expelled material concentrated in small tubes at the plasma edge, following the magnetic field lines, whereas no corresponding structures were observed for colder Ohmic plasmas. Strongly enhanced particle loss is also caused by the ELM triggered by each pellet during type-I ELMy *H*-mode plasmas [4].

A further benefit of the HFS launch becomes obvious from video observations of the pellet path as shown in Fig. 4 for the same discharge as in Fig. 2. There is a striking difference in the pellet penetration depths Δ and ablation traces between LFS [4(a)] and HFS pellets [4(b)]. Whereas LFS penetration is rather low [$\Delta \approx 8$ cm in Fig. 4(a)], significantly deeper penetration [$\Delta \approx 19$ cm in Fig. 4(b)] is found with HFS pellets. This strong difference cannot be wholly attributed to different local target plasma conditions or different flux tube spacings (Shafranov shift); we estimate that these effects yield an enhancement of Δ with HFS pellets less than 1.6 times as large as the LFS values. Whereas LFS pellet penetration depths are in agreement with published ablation scalings, HFS pellets were found to penetrate considerably deeper

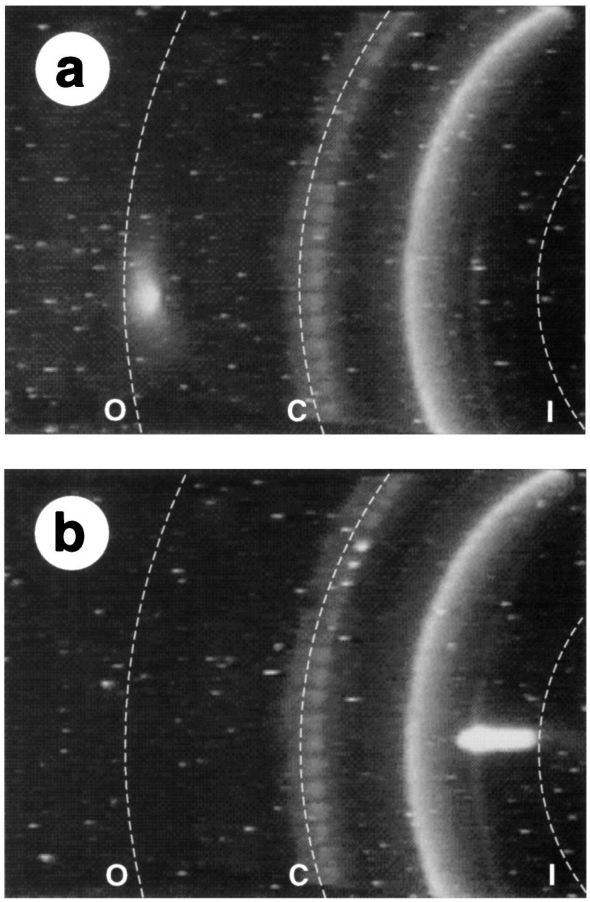

FIG. 4. Video pictures showing the complete pellet ablation traces recorded with a CCD camera (20 ms integration time for each frame; location given in Fig. 1) for the (a) 6th LFS pellet and for the (b) 5th HFS pellet of Fig. 2. Inner (right) and outer (left) divertor strike points can be seen in the background, positions of the plasma center (*C*), outer (*O*), and inner (*I*) plasma boundaries as calculated by a plasma equilibrium identification code are indicated by dashed lines.

into the plasma. We calculate Δ as 6–9 cm for the LFS and Δ as 9–14 cm for the HFS pellets, using an empirical scaling [8]. Obviously, an additional shielding mechanism must be responsible for the enhanced Δ of HFS pellets. Like LFS injection [4], pellets injected from the HFS into an *H*-mode plasma trigger ELMs.

The strong asymmetry in ε_f between shallow LFS and HFS injection is obviously a consequence of toroidal curvature, which, in principle, can affect the ultimate pellet mass deposition profile in different ways. Clearly, the asymmetry cannot be caused after the pellet mass is evenly distributed over magnetic flux surfaces (even in the presence of asymmetric turbulence), since at this time the information about the pellet launch position has already been lost. Therefore, the key process must happen on a time scale comparable to or shorter than the pellet plasma expansion time along field lines over a connection length $\pi q R_0$ between HFS and LFS, i.e., less than a few hundred microseconds [9].

Though this early, highly dynamic phase is extremely complex, a simple qualitative model may help one to understand the most important mechanisms: As shown in [9], the plasma pressure can strongly rise inside the pellet ablation cloud within a few μs. Heat is transported to the ablation cloud along field lines mainly by hot electrons, while the expansion of the cloud in the opposite direction is determined by the much slower ion acoustic velocity. Thus, the pellet ablation cloud acts as an energy sponge, and a localized high-β plasmoid is formed. In fact, for typical LFS injection cases we estimate—by assuming dimensions of the ablation clouds as observed by high-speed photographic techniques [10] and adopting our measured ablation rates—that β increases to unity within a few μs at maximum P_{NI}. This diamagnetic high-β plasmoid represents a rather extreme, localized perturbation of the initially axisymmetric tokamak equilibrium, it is a source of instabilities, and, as the key element with respect to the observed HFS vs LFS asymmetry, it is rapidly accelerated in the positive major radius direction until a new three-dimensionally distorted equilibrium is established (acceleration $a = 4\gamma kT^*/(mR)$ [11] where γ is the adiabaticity coefficient, kT^* the plasmoid temperature, m the ion mass, and R the major radius). These assumptions are consistent with high-speed framing camera observations performed at TEXT [10], where an ablation cloud velocity of about 4×10^3 m/s to the LFS is reported.

As a crude estimate of the lower limit for the time needed to set up the required Pfirsch-Schlüter currents or to short out polarization electric fields, we may take the shear Alfven transit time over one connection length in the hot background, which is of the order of 10 μs. In comparison, the β decay caused by toroidal expansion is an order of magnitude slower, while perpendicular diffusion may result in a β decay time of tens of μs, depending on the degree of local turbulence. Altogether, a moderate-β plasmoid equilibrium may not be established before a few tens of μs after pellet passage. Assuming, for example, an average plasmoid temperature of 10 eV during a nonequilibrium phase of 20 μs for high P_{NI}, the plasmoid would be captured only after a major radius displacement of about 30 cm, this being of the order of typical pellet penetration depths.

This model provides a rather natural explanation of our experimental results: With LFS injection, part of the plasmoid nucleus may be quickly lost, while the remaining pellet ablation halo is captured some distance shifted to the low-field side from its birthplace [7]. A strong variation of ε_f with plasma and pellet parameters is expected and observed (Fig. 3). In contrast, even with shallow HFS injection, the drift force (and pellet mass inertia) is directed into the plasma, and (with ELM triggering neglected) nearly perfect absorption is to be expected rather independently of the system parameters, as observed. Even the enhanced pellet shielding and penetration are qualitatively understood since some earlier ablated material can overturn the pellet being captured in front of it and causing enhanced pellet shielding and some plasma precooling there.

In summary, we have demonstrated that HFS pellet injection allows for efficient particle refuelling of hot, high confinement plasmas relevant for next generation fusion experiments. The advantage over standard LFS injection seems to originate from the toroidal curvature, which tends to expel the diamagnetic ablation cloud from the LFS, while the same effect is highly beneficial for bulk refuelling from the HFS.

[1] N. Greenwald *et al.,* Nucl. Fusion **28**, 2199 (1988).
[2] S. L. Milora, W. A. Houlberg, L. L. Lengyel, and V. Mertens, Nucl. Fusion **35**, 657 (1995).
[3] A. Carlson *et al.,* in *Controlled Fusion and Plasma Heating, Proceedings of the 15th European Conference, Dubrovnik, 1988* (European Physical Society, Geneva, 1988), Vol. 12B, Part III, p. 1069.
[4] P. T. Lang *et al.,* Nucl. Fusion **36**, 1531 (1996); corrigendum Nucl. Fusion **37**, 567 (1997).
[5] C. A. Foster *et al.,* Nucl. Fusion **17**, 1067 (1977).
[6] V. Mertens *et al.,* in *Controlled Fusion and Plasma Physics, Proceedings of the 23rd European Conference, Kiev, 1996* (European Physical Society, Geneva, 1996).
[7] L. R. Baylor *et al.,* Nucl. Fusion **32**, 2177 (1992).
[8] K. Büchl, G. C. Vlases, W. Sandmann, and R. S. Lang, Nucl. Fusion **27**, 1939 (1987).
[9] M. Kaufmann, K. Lackner, L. Lengyel, and W. Schneider, Nucl. Fusion **26**, 171 (1986).
[10] R. D. Durst *et al.,* Nucl. Fusion **30**, 3 (1990).
[11] L. L. Lengyel, Nucl. Fusion **17**, 805 (1977).